Published in final edited form as:
J Mol Biol. 2008 March 7; 376(5): 1334–1347. doi:10.1016/j.jmb.2007.12.048.

Structural Insights Into Ribosome Recycling Factor Interactions with the 70S Ribosome

Raj D. Pai[1], **Wen Zhang**[2], **Barbara S. Schuwirth**[2,3], **Go Hirokawa**[4,5], **Hideko Kaji**[4], **Akira Kaji**[6], and **Jamie H.D. Cate**[1,2,7]

[1] Department of Molecular and Cell Biology, University of California, Berkeley, CA 94720, USA

[2] Department of Chemistry, University of California, Berkeley, CA 94720, USA

[4] Department of Biochemistry and Molecular Biology, Thomas Jefferson University, Philadelphia, PA 19107

[6] Department of Microbiology, University of Pennsylvania School of Medicine, Philadelphia, PA 19104

[7] Physical Biosciences Division, Lawrence Berkeley National Laboratory, Berkeley, CA 94720, USA

SUMMARY

At the end of translation in bacteria, ribosome recycling factor (RRF) is used together with Elongation Factor G (EF-G) to recycle the 30S and 50S ribosomal subunits for the next round of translation. In x-ray crystal structures of RRF with the *Escherichia coli* 70S ribosome, RRF binds to the large ribosomal subunit in the cleft that contains the peptidyl transferase center (PTC). Upon binding of either *E. coli* or *T. thermophilus* RRF to the *E. coli* ribosome, the tip of ribosomal RNA helix H69 in the large subunit moves away from the small subunit toward RRF by 8 Å, thereby disrupting a key contact between the small and large ribosomal subunits, termed bridge B2a. In the ribosome crystals, the ability of RRF to destabilize bridge B2a is influenced by crystal packing forces. Movement of H69 involves an ordered to disordered transition upon binding of RRF to the ribosome. The disruption of bridge B2a upon RRF binding to the ribosome seen in the present structures reveals one of the key roles that RRF plays in ribosome recycling, the dissociation of 70S ribosomes into subunits. The structures also reveal contacts between Domain II of RRF and protein S12 in the 30S subunit that may also play a role in ribosome recycling.

Introduction

While peptide bond formation is catalyzed by the ribosome, many steps in the translation cycle depend on accessory proteins. At the end of translation, when the stop codon of messenger RNA (mRNA) occupies the ribosomal aminoacyl-tRNA acceptor site (A site), release factors bind to the A site and stimulate hydrolysis of peptidyl tRNA in the peptidyl–tRNA binding site (P site) thereby forming a post-termination complex (Figure 1)[1]. Bacteria use ribosome recycling factor (RRF) to aid in disassembling the post-termination complex into its constituent ribosomal small (30S) and large (50S) subunits, plus mRNA and free tRNA so they can be

[3]Present address: Cancer research UK Clare Hall Laboratories, London Research Institute, Blanche Lane, South Mimms, Potters Bar, Herts EN6 3LD, UK
[5]Present address: National Cardiovascular Institute, Osaka, Japan

reused in the next round of translation[2, 3]. Protein synthesis is dramatically reduced upon loss of RRF *in vivo*[4–6] and in the absence of RRF *in vitro*[7]. Binding of RRF to the post-termination complex occurs once the ribosome has adopted the ratcheted state (Figure 1)[8–10]. The GTPase elongation factor G (EF-G) then binds to the ribosome and together with RRF causes GTP-dependent dissociation of the 30S and 50S subunits[3, 9, 11, 12].

Crystal and solution structures of RRF from several different organisms show that it is composed of two domains that adopt an "L" configuration[13–19]. Domain I of RRF is composed of a three-helix bundle (Figure 2) that interacts with the large subunit of the ribosome[20–22]. Domain II consists of a β/α/β-sheet motif that is known to be crucial in the function of RRF and EF-G during recycling[23–25]. Domain II is attached to the Domain I by a highly flexible linker sequence (Figure 2)[18, 26, 27]. Despite these structural, biochemical and genetic results, the molecular basis for RRF function in ribosome recycling remains to be elucidated at high resolution.

Although the overall shape of RRF resembles that of a tRNA, hydroxyl radical probing and cryo-EM structures indicate that RRF binds to the ribosome in a completely different fashion than tRNAs[21, 22]. These studies of RRF bound to the empty ribosome showed that RRF is positioned in the cleft of the 50S subunit that contains the peptidyl transferase center, and is close to two key elements of the ribosome—23S rRNA helix H69 of the 50S subunit and 16S rRNA helix h44 of the 30S subunit [21, 22, 28, 29]. Helix H69 in the ribosome is a phylogenetically conserved RNA hairpin in 23S rRNA of the 50S subunit that forms a critical inter-subunit bridge, termed bridge B2a, with helix h44 in 16S rRNA of the 30S subunit[30–32]. Deletion of helix H69 results in a dominant lethal phenotype and hampers subunit association in the absence of tRNA, even at magnesium ion concentrations as high as 20 mM[33]. Chemical modifications of specific nucleotides in H69 also hinder 70S ribosome formation[34, 35]. Cryo-EM studies of an RRF/70S ribosome binary complex suggest that RRF Domain II is also in close proximity to 16S rRNA helix h44 and ribosomal protein S12 in the 30S subunit[22].

The position of RRF binding to the ribosome was revealed in more detail by a 3.3 Å crystal structure of an RRF variant containing only Domain I bound to the *Deinococcus radiodurans* 50S subunit[20]. This structure revealed that RRF binding perturbs the position of helix H69, which interacts with helix h44 in the small subunit in the context of the intact ribosome to form intersubunit bridge B2a[30–32]. However, it is not clear how well this structure reflects the steps of ribosome recycling that accompany separation of the two ribosomal subunits. In biochemical experiments, RRF binds with 6-fold higher affinity to the 70S ribosome compared to the 50S subunit[36, 37], suggesting that stable RRF association with the isolated 50S subunit may not play a physiological role[10]. Furthermore, RRF bound to the 50S subunit is not released by EF-G[38]. In a recent 3.5 Å crystal structure of *T. thermophilus* RRF bound to a *T. thermophilus* 70S ribosomal complex containing a stop codon in the A site and a transfer RNA anticodon stem-loop in the P site and $tRNA^{fMet}$ in the E site (hereafter named 70S ribosome/ASL/RRF complex) no movement of H69 was seen, when compared to other 70S ribosome structures. It was therefore suggested that movement observed in the earlier 50S subunit structure[20] may not play a role in the function of RRF[28].

In contrast, we showed that RRF from *T. thermophilus* induces H69 to move away from the subunit interface in certain contexts[29]. In order to further probe the effects of RRF on H69 dynamics, we have now determined structures of the *E. coli* 70S ribosome complexed with either *E. coli* or *T. thermophilus* RRF, both of which function on the *E. coli* ribosome[39]. Notably, RRF from both species induces specific conformational changes in helix H69 in the 50S subunit of ribosome I in the *E. coli* crystals that likely contribute to ribosome recycling. Upon RRF binding to the ribosome, helix H69 undergoes an ordered to disordered transition.

The present structures of *T. thermophilus* RRF with the *E. coli* ribosome also reveal direct interactions between Domain II of RRF and protein S12 in the 30S subunit. These structural results are compared to recent cryo-EM reconstructions of RRF bound to the ribosome[10, 22].

RESULTS

Binding of *T. thermophilus* and *E. coli* RRF to the *E. coli* ribosome

The unliganded 70S ribosome is a known substrate for RRF and EF-G, and these factors also mobilize stored ribosomes for translation *in vivo*[3, 5, 6]. In cryo-EM reconstructions, RRF binds to the vacant ribosome in either the ratcheted or unratcheted state[22]. We therefore used crystals of the *E. coli* 70S ribosome, which are in the unratcheted state, for soaking experiments to form 70S ribosome/RRF complexes for structure determination (Figure 3A). The 70S ribosome crystals contain two ribosomes per asymmetric unit (referred to as ribosome I and ribosome II) that have different crystal packing environments[32]. Therefore the crystals provide two views of the ribosome in each structure determined.

Previous biochemical data indicated that *T. thermophilus* RRF functions almost identically to *E. coli* RRF on *E. coli* ribosomes[39] provided that EF-G from *T. thermophius* is used. Therefore, complexes of the 70S ribosome with either *E. coli* or *T. thermophilus* RRF bound to the *E. coli* ribosome were initially compared at 6 Å resolution (Figure 3). At this resolution, no significant structural differences were observed in Domain I of RRF bound to either ribosome I or II. However, at lower signal to noise levels in F_{obs} - F_{obs} difference electron density maps, *T. thermophilus* RRF showed slightly more density for Domain II, when compared to maps of the *E. coli* factor (Figure 3B, 3C). A direct comparison between the *E. coli* and *T. thermophilus* RRF complexes revealed positive difference electron density for RRF Domain I, reflecting the higher stoichiometric binding of the *T. thermophilus* factor in the crystals (Figure 3D). This may indicate a naturally higher affinity of *T. thermophilus* RRF for the *E. coli* ribosome compared to *E. coli* RRF. Alternatively, the difference in binding stoichiometry could be due to the longer crystal soaking times with *T. thermophilus* RRF used in these experiments. Despite the possible differences in binding stoichiometry, the qualitatively identical results observed with either *E. coli* or *T. thermophilus* RRF bound to the *E. coli* ribosome indicates that the results obtained with *T. thermophilus* RRF reflect the general properties of RRF, and not species-specific effects.

As a control to ensure that crystal-packing forces would not affect the results of soaking RRF into preformed crystals, *E. coli* RRF was co-crystallized with the 70S ribosome. Although the resulting crystals diffracted x-rays to only 7 Å, the position of RRF in ribosome II compared to *T. thermophilus* RRF binding in soaked crystals was essentially indistinguishable (Figure 4). Furthermore, difference electron density for *E. coli* RRF Domain I could be clearly identified, whereas difference electron density for *E. coli* RRF Domain II was somewhat weaker, as observed in soaking experiments. In ribosome I, the difference electron density was not as clear, suggesting that RRF bound more weakly to ribosome I. We therefore focused our efforts on determining high-resolution structures of *T. thermophilus* RRF bound to the 70S ribosome by soaking RRF into pre-grown 70S ribosome crystals.

RRF and Helix H69 of the Ribosome

When *T. thermophilus* RRF is bound to ribosome I in the crystals, helix H69 (hereafter termed RRF-I and H69-I, respectively) moves away from the subunit interface and its helical pitch becomes overwound (Figure 5)[29]. Comparing H69-I in the apo-ribosome structure[32] to H69-I in the RRF-bound structure indicates that the majority of the factor-induced changes occur between nucleotides C1905 and G1929 (Figure 6). A kink develops at nucleotide G1906 that

extends helix H69 toward the three-helix bundle of RRF (Figure 5, Figure 6). Furthermore, nucleotides C1908, C1909, and C1920 contribute to an overwinding of the helical pitch that positions the tip of H69 close to the three-helix bundle of RRF-I (Figure 6).

The structure indicates that helix H69-I undergoes an ordered to disordered transition upon binding of RRF. In F_{obs} - F_{obs} difference electron density maps truncated to low resolution (6 Å), the difference electron density reveals that helix H69-I is displaced from helix h44 of the small subunit towards RRF by approximately 8 Å (Figure 5A)[29]. However, in difference maps calculated to higher resolution (3.5 Å) the positive difference electron density is broken up, indicating that helix movement also results in a disordering in the helix (Figure 5B). Further evidence of the disordered nature of helix H69-I in the presence of RRF comes from analysis of the crystallographic temperature factors after structure refinement (Figure 6)[40]. In the apo-70S ribosome structure, helix 69 has moderately high temperature factors in the helical region, and becomes disordered only at the tip of H69, around nucleotide C1914. However upon RRF binding to ribosome I, the temperature factors of H69-I increase throughout the helix starting at C1908 and continuing through U1923, revealing the disordered nature of the helix.

Although H69 is not well ordered in the structure of ribosome I with RRF bound, the structural model suggests that Domain I of RRF-I interacts with H69-I through a small neutral patch on the tip of the helix. RRF amino acids H23, V20 and S17, which lie on one face of α-helix 1 in Domain I, interact with the minor groove of nucleotides C1914 and Ψ1917. In addition, amino acid N24 in RRF may interact with nucleotide C1914, potentially favoring the RRF induced conformational change of H69-I (Figure 5C, Table 2).

The conformation of H69 in ribosome II (H69-II) in the RRF complex is strikingly different from that in ribosome I. RRF is unable to dissociate H69-II from the subunit interface (Figure 5D), in contrast to its effect on ribosome I. The interface of ribosome II is stabilized in the crystals in such a way that RRF may be unable to drive the helix H69-II conformational change as effectively as in ribosome I. At the present resolution, we are unable to provide a quantitative surface area analysis of the interface between the 30S and 50S subunits in the two ribosomes that may explain the difference. However in the apo-70S ribosome structure, clear differences in the packing near bridge B2a could be seen in the two ribosomes[32]. Notably, movement of H69 was detected in ribosome II when complexes of the 70S ribosome with RRF and gentamicin at different concentrations were compared[29].

The ability of RRF to displace H69-I is not species-dependent, i.e. it is not unique to *T. thermophilus* RRF acting on the *E. coli* ribosome. When *E. coli* RRF was soaked into the 70S ribosome crystals, *E. coli* RRF was able to displace H69 in ribosome I but not in ribosome II (Figure 5E, Figure 3B). Additionally when *E. coli* RRF was co-crystallized with the 70S ribosome, RRF displaced H69 in ribosome I but not ribosome II (Figure 5F, Figure 4B). These results indicate that ribosomes in the crystals respond to RRF binding in a reproducible manner, regardless of the source of RRF.

Interactions of RRF Domain I with the 50S subunit

RRF Domain I binds to the A- and P-site cleft of the 50S subunit in both ribosomes I and II, similarly to what was observed in the structure of RRF Domain I bound to the 50S subunit[20] and bound to the 70S ribosome[22]. This binding does not cause any drastic conformational changes in the ribosome, aside from movement of helix H69 in ribosome I. There is no significant difference between Domain I of RRF-I and RRF-II in the crystallographic asymmetric unit (Cα rmsd 0.5 Å). Both structures of RRF Domain I are also highly similar to Domain I of RRF bound to the 50S subunit from *D. radiodurans* (Cα rmsd 1.45 Å) and in the 70S ribosome/ASL/RRF complex[28] (Cα rmsd .96 Å).

The three-helix bundle that makes up Domain I of RRF contains numerous positively charged amino acids that interact with various parts of the backbone of 23S RNA in the 50S subunit (Table 2). Compared to the structure of RRF Domain I with the 50S *D. radiodurans* subunit, and to the 70S ribosome/ASL/RRF complex[28] the 70S structures presented here reveal similar interactions with 23S RNA helix H71 and nucleotides in helix H80. At the tip of the three-helix bundle in RRF, amino acids 147–150 likely form hydrogen bonds and hydrophobic interactions with nucleotides G2253-G2255 (termed the P-loop) in 23S RNA[41] (See Figure 7A, Table 2). There is no electron density for the N-terminus for protein L27, which resides near the binding position of RRF[20, 28].

Although RRF binds to both ribosomes as evidenced by difference electron density for RRF Domain I (Figure 5, Figure 7), a comparison of difference electron density maps shows stronger density for RRF Domain I in the RRF complex with ribosome II compared to that with ribosome I (not shown). This is further confirmed by comparison with difference density maps of the ribosome co-crystallized with RRF, where RRF bound to ribosome II also has significantly more density than RRF-I (not shown). Additionally, $3F_{obs}$ -$2F_{calc}$ difference electron density maps have significantly more density for RRF-II compared to RRF-I (Figure 7).

Domain II of *Thermus Thermophilus* RRF

In our initial soaking experiments, we observed some electron density for *T. thermophilus* RRF Domain II in 6 Å F_{obs} - F_{obs} difference maps when RRF is bound to ribosome II (Figure 3). However, in $3F_{obs}$ - $2F_{calc}$ difference electron density maps at 3.3 Å resolution, no density is visible for RRF Domain II (Figure 7). Notably, in the higher resolution data truncated to 6 Å resolution, electron density is observed for Domain II (Figure 8A), indicating that this domain of RRF is inherently mobile on the ribosome. RRF Domain II appears more readily in ribosome II compared to ribosome I, possibly as a result of the tighter packing of ribosome II[32].

Protein S12 in the 30S subunit has been shown to be important for mRNA and tRNA translocation on the ribosome and may buttress the pivot point for the ratcheted state of the ribosome observed in cryo-EM reconstructions[9]. Recent low-resolution cryo-EM reconstructions of the post-termination complex with RRF suggest a possible Domain II interaction with protein S12[9, 22]. In these reconstructions, *E. coli* RRF amino acids 83–90 interact with amino acids 34–37 and 74–76 of *E. coli* protein S12. In contrast, RRF Domain II in the 70S ribosome/ASL/RRF complex does not seem to make significant contacts with protein S12[28]. In the present structure of ribosome II, amino acids 84–92 and 102–107 of *T. thermophilus* RRF Domain II are close enough to interact with amino acids 35–40, 48–50 and 71–76 of protein S12 (Figure 8).

To test the specificity of the interaction, we analyzed the predicted contacts between RRF and protein S12 through evolutionary trace (ET) methodology[42]. Evolutionary trace methods partition sequences of a particular protein family into different groups originating from a common node in a phylogenetic tree. Construction of consensus sequences from each group allows identification of conserved residues that can be mapped to known structures, thereby identifying potential interaction sites within or between proteins[43]. Therefore ET methodology can be applied to determine whether an observed crystallographic interface is functionally relevant or simply a crystallization artifact[44, 45]. The amino acids in the putative contact between RRF and protein S12 that are conserved and class-specific by ET analysis cluster around the interface area (Figure 8C), consistent with these contacts representing functional interactions.

Discussion

RRF and EF-G are known to dissociate vacant 70S ribosomes into subunits *in vitro*[3], which may reflect a role for RRF in reactivating 70S ribosomes that have been sequestered in an inactive state during stationary phase or stress[3, 5, 6]. While no biochemical experiments have yet been carried out to determine how proteins that sequester the ribosome during stress (i.e protein Y or RMF[46, 47]) affect the activity of RRF, genetic experiments performed using RRF temperature sensitive mutants provide evidence of the essential nature of this protein during recovery from the lag phase[5]. In this paper, the structure of the apo-70S *E. coli* ribosome in complex with *T. thermophilus* RRF has been determined to 3.3 Å resolution (Table 1), and compared to lower resolution structures of *T. thermophilus* or *E. coli* RRF bound to the *E. coli* ribosome.

A significant difference exists between the present structures, RRF Domain I bound to the *D. radiodurans* 50S subunit[20], and the 70S ribosome/ASL/RRF complex[28] regarding the motion of helix H69 in the 50S subunit (Figure 5B). While Wilson *et al.* reported a 20 Å displacement of the tip of helix H69 away from the 50S subunit upon binding of RRF, the 70S ribosome/RRF complexes reported here indicate that the tip of H69 in ribosome I moves in the opposite direction, i.e. away from h44 in the 30S subunit by 8 Å, thereby disrupting intersubunit bridge B2a. As mentioned above, RRF has a weaker affinity for the isolated 50S subunit than to the 70S ribosome[36, 37] and recent cryo-EM reconstructions suggest movement of RRF to the P site on the 50S subunit after the 70S ribosome is dissociated[10]. Thus, in the structure of RRF Domain I with the 50S subunit[20], the interactions between RRF Domain I and H69 may not represent a physiological state. An important observation in this context is that RRF bound to isolated 50S subunits is not released by EF-G while RRF bound to the 70S ribosome is released by EF-G[38], supporting the notion that RRF bound to the isolated 50S subunit may not represent a physiological state of RRF interactions with the ribosome. However, aside from H69 movement, it is important to note that in the 50S subunit structure with RRF Domain I, the interactions between RRF Domain I with the rest of the 50S subunit correspond closely to what is observed in the 70S ribosome structures with RRF.

In the 70S ribosome/ASL/RRF complex, RRF does not induce movement of helix H69 away from helix h44, and RRF does not interact with H69[28]. This result is consistent with the effects of RRF on ribosome II in the *E. coli* ribosome crystals used here, and may reflect the stabilizing influence of crystal packing on the ribosome in these cases. In contrast, RRF binding to the ribosome causes H69 to become disordered in cryo-EM reconstructions of complexes assembled under more physiological ionic conditions and temperature[22]. Additional evidence for an important role for helix H69 in RRF-dependent ribosome recycling comes from experiments in which deletion of helix H69 from the ribosome allows subunit dissociation to occur in the absence of RRF[33]. Finally, we recently found that in structures of the 70S ribosome with RRF and the antibiotics gentamicin or paromomycin, known inhibitors of ribosome recycling[36], the antibiotics stabilize bridge B2a by binding to helix H69[29] in addition to their well-known binding site in helix h44[31], thereby preventing H69 movement towards RRF[29].

The conformational change in H69-I induced by RRF in the unratcheted state of the ribosome observed here indicates that RRF inherently destabilizes contacts between H69 and the 30S subunit in intersubunit bridge B2a. As opposed to RRF binding to ribosome II or to the 70S/ASL/RRF complex[28], RRF binding to ribosome I seems to overcome the crystal packing forces that stabilize H69 at the ribosomal interface. Notably, RRF from both *E. coli* and *T. thermophilus* is capable of destabilizing bridge B2a in the *E. coli* ribosome crystals, showing that the movement of H69-I observed here is not an artifact of using a heterologous system. The ability of RRF to destabilize bridge B2a prior to EF-G binding is consistent with biochemical results in which RRF without EF-G assistance has weak intrinsic ribosome

recycling activity[10]. Weakening of bridge B2a by RRF may therefore play an essential physiological role to enhance EF-G dependent steps in ribosome recycling.

It is the combined action of RRF and EF-G that is necessary to lead to rapid subunit dissociation[1]. While the precise mechanism has not been elucidated, a recent low-resolution cryo-EM reconstruction suggests that RRF could potentially move from its initial binding site to the P site on the 50S subunit that would conflict with a number of additional bridges[10]. GTP hydrolysis by EF-G may be critical for providing the necessary energy to relocate RRF into this second position, concomitant with subunit dissociation.

Upon binding of RRF Domain I to the *D. radiodurans* 50S subunit, there was a noticeable ordering of the N-terminus and the loop between α-helices III and IV of ribosomal L27[20]. In contrast, the N-terminus of L27 in the apo-70S ribosome structures[31, 32] and in the 70S ribosome/RRF structures presented here is disordered. Notably, although L27 and Domain I are close to each other, no significant effects of RRF on the conformation of L27 were seen in the *T. thermophilus* 70S ribosome/ASL/RRF complex[28] when compared to the high-resolution *T. thermophilus* 70S ribosome structure[31]. Nevertheless, it would be interesting to examine whether mutations in protein L27 affect the activity of the ribosome during recycling.

The interaction of RRF Domain II with protein S12 may also play an important role in driving subunit dissociation by EF-G[9, 22]. In the present structures, RRF Domain II is disordered in ribosome I, and only weakly positioned in ribosome II (Figure 3› Figure 7› Figure 8). This indicates that RRF Domain II is inherently mobile on the 70S ribosome, consistent with solution structural studies of RRF[18]. The 70S ribosome/ASL/RRF[28] complex, as well as the recent cryo-EM reconstruction of RRF bound to the ribosome[10] further confirms the mobility of Domain II on the ribosome. Despite the inherent mobility of RRF Domain II, the electron density for RRF Domain II in ribosome II provides evidence for contacts between RRF and protein S12 that are predicted to be functionally important, based on evolutionary trace analysis (Figure 8). This is the highest resolution demonstration of the actual interaction between RRF Domain II and S12 (approximately 6 Å). Notably, in the ratcheted state of the ribosome (Figure 1B), Gao *et al*.[9] showed the interaction of these two components at lower resolution in cryo-EM reconstructions, and Barat *et al*. also detect a similar conformation of RRF (termed IIb) [10]. At present no biochemical experiments have been performed to test the effects of mutations in protein S12 or RRF at the observed interface between the proteins. One biological hint supporting the importance of the conservation of these sequences comes from a recent study where mutations in S12 resulted in the overproduction of the antibiotic actinorhodin in *Streptomyces coelicolor*. When the expression of ribosome translation factors was quantified, only RRF levels had increased during the stationary phase. Conversely, overexpression of RRF increased the production of the antibiotic significantly[48]. Future high–resolution structures of other ribosome recycling states should help to elucidate the mechanism of ribosome recycling, and the role of putative interactions between protein S12 and RRF.

RRF presents an extremely appealing target for drug design since it does not exist in the cytoplasm of eukaryotes, but is essential in bacteria[4]. Therefore, a better understanding of its interaction with the ribosome and the dynamic nature of H69 may be useful in designing antibiotics that specifically target ribosome recycling. Further experiments to test antibiotic binding and which amino acids in RRF contribute the most to helix H69 dynamics will greatly improve our understanding of antibiotic inhibition of ribosome recycling.

Methods

Crystallization and RRF binding

Ribosomes from *E. coli* strain MRE 600 were purified as previously described[32]. Crystals were grown at 4 °C using microbatch 96 well plates and buffers containing 11% 2-methyl-2, 4-pentanediol (MPD), 2% PEG 8000, 33 mM magnesium chloride, 350 mM ammonium chloride, 1 mM spermine, 0.5 mM spermidine, 10 mM Tris (pH =7.5) and 0.25 mM EDTA. *T. thermophilus* and *E. coli* RRF were purified as previously described[39].

In order to form the RRF/70S ribosome binary complexes, RRF (10 μM) was soaked into pre-grown apo-70S ribosome crystals. A modified form of cryo-protectant containing 20% 2-methyl-2, 4-pentanediol (MPD), 3% PEG 8000, 24% PEG 400, 35 mM magnesium chloride, 350 mM ammonium chloride, 1 mM spermine, 0.5 mM spermidine, and 60 mM HEPES (pH 7.0) was used in soaking experiments. Initial attempts to soak RRF into crystals overnight for twelve hours to form the binary complex resulted in only a modest resolution of diffraction (Table 1), and weak electron density for RRF binding to ribosome I. In order to increase the stoichiometry of RRF binding to the ribosome in the crystals, RRF was soaked into crystals over a period of several days, with cryo-protectant at intermediate concentrations. The soaking time lasted for a minimum of three days but no more than four, before stabilizing crystals in the cryo-protectant above and flash freezing the crystals in liquid nitrogen.

Data Collection

X-ray diffraction data were measured at the Advanced Light Source at Beamline 12.3.1, which is equipped with an ADSC Q315 area detector. A modified strategy algorithm was used to optimize the data collection efficiency when collecting from many different crystals[32]. Fourteen crystals were merged to complete the diffraction data for the structure of *T. thermophilus* RRF bound to the ribosome at 3.3 Å resolution. Data were processed using Denzo/Scalepack[49] and converted to diffraction amplitudes using Truncate[50].

Structure refinement and electron density map calculations

F_{obs} - F_{obs} difference electron density maps between the RRF/70S binary complex and the *E. coli* apo-70S ribosomes were constructed using structure factor phases derived from the Pirate density modification program[51]. *T. Thermophilus* RRF (PDB ID code: 1EH1)[19] was then docked into the difference density maps by following the clear density of the three-helix bundle of Domain I using O[52]. Side chains were modeled where electron density was clearly present. While we cannot accurately model the side chains of every residue at the present resolution of 3.3 Å for Domain I, large amino acids were clearly visible and could be accurately refined. Rigid body, torsional, and B-factor refinement were then performed using the CNS program (Table 1)[40]. The Cα positions of RRF Domain II were maintained as a rigid body during refinement, due to the inherent flexibility in this region of RRF. F_{obs} - F_{obs} difference maps shown in the figures used the data sets presented in Table 1, as well as diffraction data from the apo-70S ribosome[32].

Evolutionary Trace analysis of protein S12 and RRF interactions

Multiple sequence alignments (MSA) of RRF and ribosomal S12 protein families were obtained from Pfam[53] through entries PF01765 and PF00164, respectively. The sequences were extracted with the corresponding sequence names for an evolutionary trace (ET) analysis. The conserved and class specific residues were analyzed with the server TraceSuite II[42]. With 20 partitions, we traced the conserved, varied (i.e. class-specific), buried and exposed residues and mapped these residues onto the structures of *E. coli* S12 and *T. thermophilus* RRF in the

context of ribosome II. Spatial clustering of important residues identified by ET analysis revealed the location of likely functional interactions between RRF and S12.

Figures

Figures were prepared using Pymol[54], and Ribbons[55].

Acknowledgments

We would like to thank K. Frankel, G. Meigs, and J. Holton at the Advanced Light Source for their help in collection of the diffraction data. R.P. would also like to further thank A. Vila-Sanjurjo, N. Endres, M. Wetzler, M. Doucleff, D. Colón-Ramos, Natasha Keith and C. Eidem for helpful comments and suggestions during the writing of this manuscript. R.P. and W.Z also wish to thank V. Berk with initial help collecting diffraction data and P. Adams for useful advice in analyzing the data. PDB coordinates for the high-resolution structure of RRF bound to the ribosome have been deposited (PDB accession codes 2QBD, 2QBE, 2QBF, 2QBG). Structure factors for the lower-resolution data are available as supplementary information from the authors.

This work was supported by US National Institutes of Health (NIH) grants GM65050 (J.H.D.C) and GM60429 (A.K.), the Nippon Paint Fund (H.K.), NIH National Cancer Institute grant CA92584 (for SIBYLS and 8.3.1 beamlines), LBNL LDRD 366851 (J.H.D.C), DE-AC03 76SF00098 (for the SIBYLS and 8.3.1 beamlines).

References

1. Hirokawa G, Demeshkina N, Iwakura N, Kaji H, Kaji A. The ribosome-recycling step: consensus or controversy? Trends Biochem Sci 2006;31:143–9. [PubMed: 16487710]
2. Hirashima A, Kaji A. Role of elongation factor G and a protein factor on the release of ribosomes from messenger ribonucleic acid. J Biol Chem 1973;248:7580–7. [PubMed: 4583357]
3. Hirokawa G, Nijman RM, Raj VS, Kaji H, Igarashi K, Kaji A. The role of ribosome recycling factor in dissociation of 70S ribosomes into subunits. RNA 2005;11:1317–28. [PubMed: 16043510]
4. Janosi L, Shimizu I, Kaji A. Ribosome recycling factor (ribosome releasing factor) is essential for bacterial growth. Proc Natl Acad Sci U S A 1994;91:4249–53. [PubMed: 8183897]
5. Janosi L, Mottagui-Tabar S, Isaksson LA, Sekine Y, Ohtsubo E, Zhang S, Goon S, Nelken S, Shuda M, Kaji A. Evidence for in vivo ribosome recycling, the fourth step in protein biosynthesis. EMBO J 1998;17:1141–51. [PubMed: 9463391]
6. Hirokawa G, Inokuchi H, Kaji H, Igarashi K, Kaji A. In vivo effect of inactivation of ribosome recycling factor - fate of ribosomes after unscheduled translation downstream of open reading frame. Mol Microbiol 2004;54:1011–21. [PubMed: 15522083]
7. Janosi L, Hara H, Zhang S, Kaji A. Ribosome recycling by ribosome recycling factor (RRF)--an important but overlooked step of protein biosynthesis. Adv Biophys 1996;32:121–201. [PubMed: 8781287]
8. Frank J, Agrawal RK. A ratchet-like inter-subunit reorganization of ribosome during translocation. Nature 2000;406:318–22. [PubMed: 10917535]
9. Gao N, Zavialov AV, Li W, Sengupta J, Valle M, Gursky RP, Ehrenberg M, Frank J. Mechanism for the disassembly of the posttermination complex inferred from cryo-EM studies. Mol Cell 2005;18:663–74. [PubMed: 15949441]
10. Barat C, Datta PP, Raj VS, Sharma MR, Kaji H, Kaji A, Agrawal RK. Progression of the ribosome recycling factor through the ribosome dissociates the two ribosomal subunits. Mol Cell 2007;27:250–61. [PubMed: 17643374]
11. Zavialov AV, Hauryliuk VV, Ehrenberg M. Splitting of the posttermination ribosome into subunits by the concerted action of RRF and EF-G. Mol Cell 2005;18:675–86. [PubMed: 15949442]
12. Peske F, Rodnina MV, Wintermeyer W. Sequence of steps in ribosome recycling as defined by kinetic analysis. Mol Cell 2005;18:403–12. [PubMed: 15893724]
13. Saikrishnan K, Kalapala SK, Varshney U, Vijayan M. X-ray structural studies of Mycobacterium tuberculosis RRF and a comparative study of RRFs of known structure. Molecular plasticity and biological implications. J Mol Biol 2005;345:29–38. [PubMed: 15567408]

14. Vijayan M. Structural biology of mycobacterial proteins: the Bangalore effort. Tuberculosis (Edinb) 2005;85:357–66. [PubMed: 16260182]
15. Kim KK, Min K, Suh SW. Crystal structure of the ribosome recycling factor from Escherichia coli. EMBO J 2000;19:2362–70. [PubMed: 10811627]
16. Nakano H, Yoshida T, Uchiyama S, Kawachi M, Matsuo H, Kato T, Ohshima A, Yamaichi Y, Honda T, Kato H, Yamagata Y, Ohkubo T, Kobayashi Y. Structure and binding mode of a ribosome recycling factor (RRF) from mesophilic bacterium. J Biol Chem 2003;278:3427–36. [PubMed: 12411440]
17. Selmer M, Al-Karadaghi S, Hirokawa G, Kaji A, Liljas A. Crystal structure of Thermotoga maritima ribosome recycling factor: a tRNA mimic. Science 1999;286:2349–52. [PubMed: 10600747]
18. Yoshida T, Uchiyama S, Nakano H, Kashimori H, Kijima H, Ohshima T, Saihara Y, Ishino T, Shimahara H, Yoshida T, Yokose K, Ohkubo T, Kaji A, Kobayashi Y. Solution structure of the ribosome recycling factor from Aquifex aeolicus. Biochemistry 2001;40:2387–96. [PubMed: 11327859]
19. Toyoda T, Tin OF, Ito K, Fujiwara T, Kumasaka T, Yamamoto M, Garber MB, Nakamura Y. Crystal structure combined with genetic analysis of the Thermus thermophilus ribosome recycling factor shows that a flexible hinge may act as a functional switch. RNA 2000;6:1432–44. [PubMed: 11073219]
20. Wilson DN, Schluenzen F, Harms JM, Yoshida T, Ohkubo T, Albrecht R, Buerger J, Kobayashi Y, Fucini P. X-ray crystallography study on ribosome recycling: the mechanism of binding and action of RRF on the 50S ribosomal subunit. EMBO J 2005;24:251–60. [PubMed: 15616575]
21. Lancaster L, Kiel MC, Kaji A, Noller HF. Orientation of ribosome recycling factor in the ribosome from directed hydroxyl radical probing. Cell 2002;111:129–40. [PubMed: 12372306]
22. Agrawal RK, Sharma MR, Kiel MC, Hirokawa G, Booth TM, Spahn CM, Grassucci RA, Kaji A, Frank J. Visualization of ribosome-recycling factor on the Escherichia coli 70S ribosome: functional implications. Proc Natl Acad Sci U S A 2004;101:8900–5. [PubMed: 15178758]
23. Janosi L, Mori H, Sekine Y, Abragan J, Janosi R, Hirokawa G, Kaji A. Mutations influencing the frr gene coding for ribosome recycling factor (RRF). J Mol Biol 2000;295:815–29. [PubMed: 10656793]
24. Zhang L, Guo P, Zhang H, Jing G. Cooperative unfolding of Escherichia coli ribosome recycling factor originating from its domain-domain interaction and its implication for function. Arch Biochem Biophys 2006;450:191–202. [PubMed: 16684502]
25. Guo P, Zhang L, Zhang H, Feng Y, Jing G. Domain II plays a crucial role in the function of ribosome recycling factor. Biochem J 2006;393:767–77. [PubMed: 16262604]
26. Nakano H, Uchiyama S, Yoshida T, Ohkubo T, Kato H, Yamagata Y, Kobayashi Y. Crystallization and preliminary X-ray crystallographic studies of a mutant of ribosome recycling factor from Escherichia coli, Arg132Gly. Acta Crystallogr D Biol Crystallogr 2002;58:124–6. [PubMed: 11752787]
27. Stagg SM, Harvey SC. Exploring the flexibility of ribosome recycling factor using molecular dynamics. Biophys J 2005;89:2659–66. [PubMed: 16055531]
28. Weixlbaumer A, Petry S, Dunham CM, Selmer M, Kelley AC, Ramakrishnan V. Crystal structure of the ribosome recycling factor bound to the ribosome. Nat Struct Mol Biol 2007;14:733–7. [PubMed: 17660830]
29. Borovinskaya MA, Pai RD, Zhang W, Schuwirth BS, Holton JM, Hirokawa G, Kaji H, Kaji A, Cate JH. Structural basis for aminoglycoside inhibition of bacterial ribosome recycling. Nat Struct Mol Biol 2007;14:727–32. [PubMed: 17660832]
30. Yusupov MM, Yusupova GZ, Baucom A, Lieberman K, Earnest TN, Cate JH, Noller HF. Crystal structure of the ribosome at 5.5 A resolution. Science 2001;292:883–96. [PubMed: 11283358]
31. Selmer M, Dunham CM, Murphy FVt, Weixlbaumer A, Petry S, Kelley AC, Weir JR, Ramakrishnan V. Structure of the 70S ribosome complexed with mRNA and tRNA. Science 2006;313:1935–42. [PubMed: 16959973]
32. Schuwirth BS, Borovinskaya MA, Hau CW, Zhang W, Vila-Sanjurjo A, Holton JM, Cate JH. Structures of the bacterial ribosome at 3.5 A resolution. Science 2005;310:827–34. [PubMed: 16272117]
33. Ali IK, Lancaster L, Feinberg J, Joseph S, Noller HF. Deletion of a conserved, central ribosomal intersubunit RNA bridge. Mol Cell 2006;23:865–74. [PubMed: 16973438]

34. Gutgsell NS, Deutscher MP, Ofengand J. The pseudouridine synthase RluD is required for normal ribosome assembly and function in Escherichia coli. RNA 2005;11:1141–52. [PubMed: 15928344]
35. Maivali U, Remme J. Definition of bases in 23S rRNA essential for ribosomal subunit association. RNA 2004;10:600–4. [PubMed: 15037769]
36. Hirokawa G, Kiel MC, Muto A, Selmer M, Raj VS, Liljas A, Igarashi K, Kaji H, Kaji A. Post-termination complex disassembly by ribosome recycling factor, a functional tRNA mimic. EMBO J 2002;21:2272–81. [PubMed: 11980724]
37. Hirokawa G, Kiel MC, Muto A, Kawai G, Igarashi K, Kaji H, Kaji A. Binding of ribosome recycling factor to ribosomes, comparison with tRNA. J Biol Chem 2002;277:35847–52. [PubMed: 12138121]
38. Kiel MC, Raj VS, Kaji H, Kaji A. Release of ribosome-bound ribosome recycling factor by elongation factor G. J Biol Chem 2003;278:48041–50. [PubMed: 12960150]
39. Raj VS, Kaji H, Kaji A. Interaction of RRF and EF-G from E. coli and T. thermophilus with ribosomes from both origins--insight into the mechanism of the ribosome recycling step. RNA 2005;11:275–84. [PubMed: 15661844]
40. Brunger AT, Adams PD, Rice LM. Recent developments for the efficient crystallographic refinement of macromolecular structures. Curr Opin Struct Biol 1998;8:606–11. [PubMed: 9818265]
41. Puglisi EV, Green R, Noller HF, Puglisi JD. Structure of a conserved RNA component of the peptidyl transferase centre. Nat Struct Biol 1997;4:775–8. [PubMed: 9334738]
42. Innis CA, Shi J, Blundell TL. Evolutionary trace analysis of TGF-beta and related growth factors: implications for site-directed mutagenesis. Protein Eng 2000;13:839–47. [PubMed: 11239083]
43. Nagarajan S, Marimuthu P. Binding site prediction of galanin peptide using evolutionary trace method. Bioinformation 2006;1:180–3. [PubMed: 17597884]
44. Thornton JM. From genome to function. Science 2001;292:2095–7. [PubMed: 11408660]
45. McCammon JA. Theory of biomolecular recognition. Curr Opin Struct Biol 1998;8:245–9. [PubMed: 9631300]
46. Agafonov DE, Kolb VA, Spirin AS. Ribosome-associated protein that inhibits translation at the aminoacyl-tRNA binding stage. EMBO Rep 2001;2:399–402. [PubMed: 11375931]
47. Wada A, Yamazaki Y, Fujita N, Ishihama A. Structure and probable genetic location of a “ribosome modulation factor” associated with 100S ribosomes in stationary-phase Escherichia coli cells. Proc Natl Acad Sci U S A 1990;87:2657–61. [PubMed: 2181444]
48. Hosaka T, Xu J, Ochi K. Increased expression of ribosome recycling factor is responsible for the enhanced protein synthesis during the late growth phase in an antibiotic-overproducing Streptomyces coelicolor ribosomal rpsL mutant. Mol Microbiol 2006;61:883–97. [PubMed: 16859496]
49. Otwinowski Z, Minor W. Processing of X-ray diffraction Data collected in oscillation mode. Methods in Enzymology 1997;276:307–326.
50. Collaborative Computational Project, N. The CCP4 suite: programs for protein crystallography. Acta Crystallographica D 1994;50:760–763.
51. Cowtan K. General quadratic functions in real and reciprocal space and their application to likelihood phasing. Acta Crystallogr D Biol Crystallogr 2000;56:1612–1621. [PubMed: 11092927]
52. Jones T, Zou J, Cowan S, Kjeldgaard M. Improved methods for building protein models in electron density maps and the location of errors in these models. Acta Crystallogr A 1991;47:110–119. [PubMed: 2025413]
53. Finn RD, Mistry J, Schuster-Bockler B, Griffiths-Jones S, Hollich V, Lassmann T, Moxon S, Marshall M, Khanna A, Durbin R, Eddy SR, Sonnhammer EL, Bateman A. Pfam: clans, web tools and services. Nucleic Acids Res 2006;34:D247–51. [PubMed: 16381856]
54. DeLano, WL. The PyMOL Molecular Graphics System. 2002. World Wide Web http://www.pymol.org
55. Carson M. Ribbons. Methods in Enzymology 1997;277:193–502.

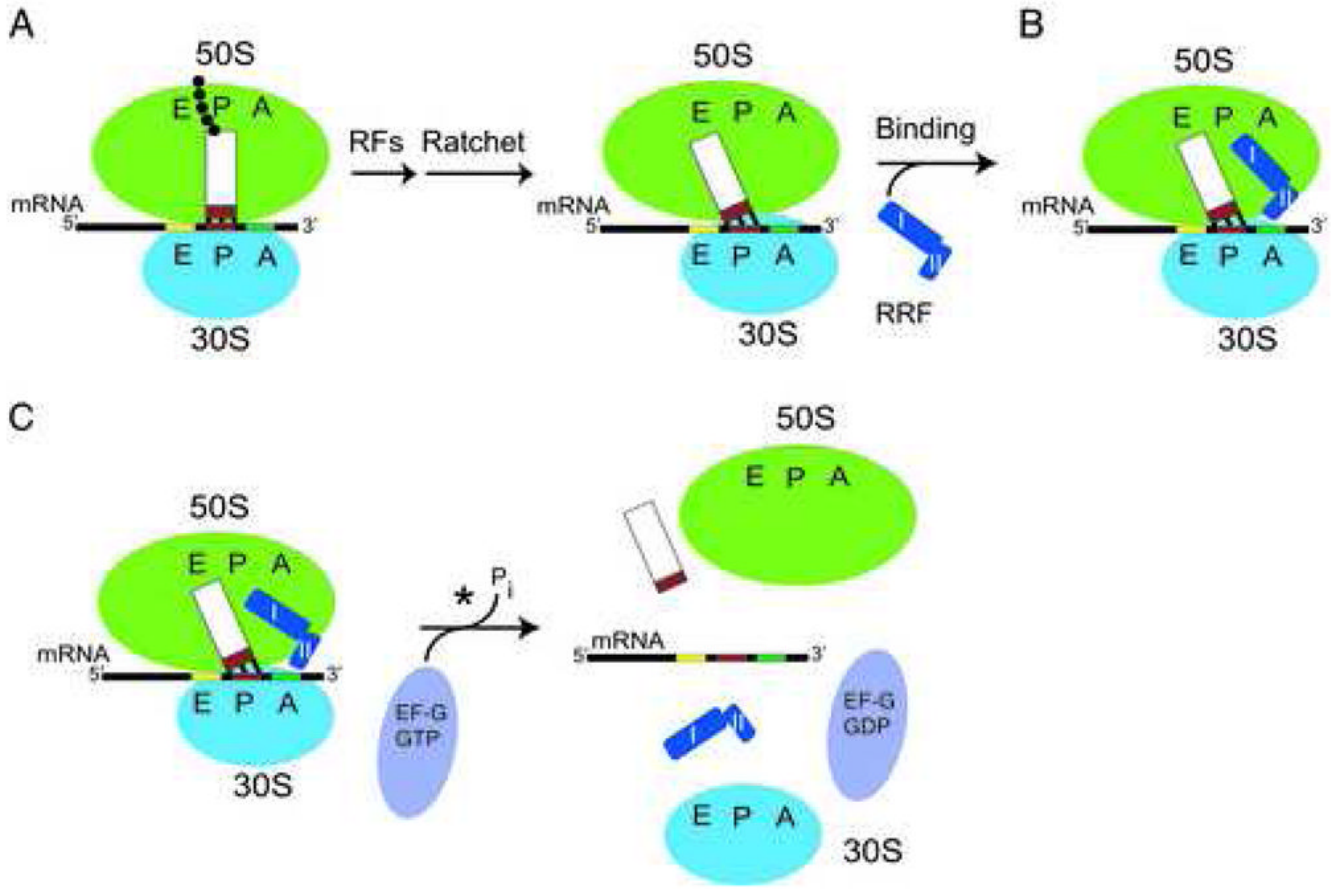

Figure 1.

Brief overview of the ribosome recycling process. (A) At the end of the translation cycle, the stop codon occupies the A site. Release Factors (RFs) hydrolyze the polypeptide from peptidyl-tRNA in the P site at this point. The ribosome then exists in a post-termination complex in the classical conformation, i.e. unratcheted state, which then converts to the ratcheted state. (B) RRF binds to the post-termination complex, in the ratcheted state of the ribosome[8–10]. (C) EF-G binding to the complex[10, 20–22, 38] coupled with GTP hydrolysis dissociates the subunits from each other as well as mRNA and tRNA[1–3, 10–12, 21, 22]. The asterisk indicates that multiple steps occur in the process of subunit dissociation.

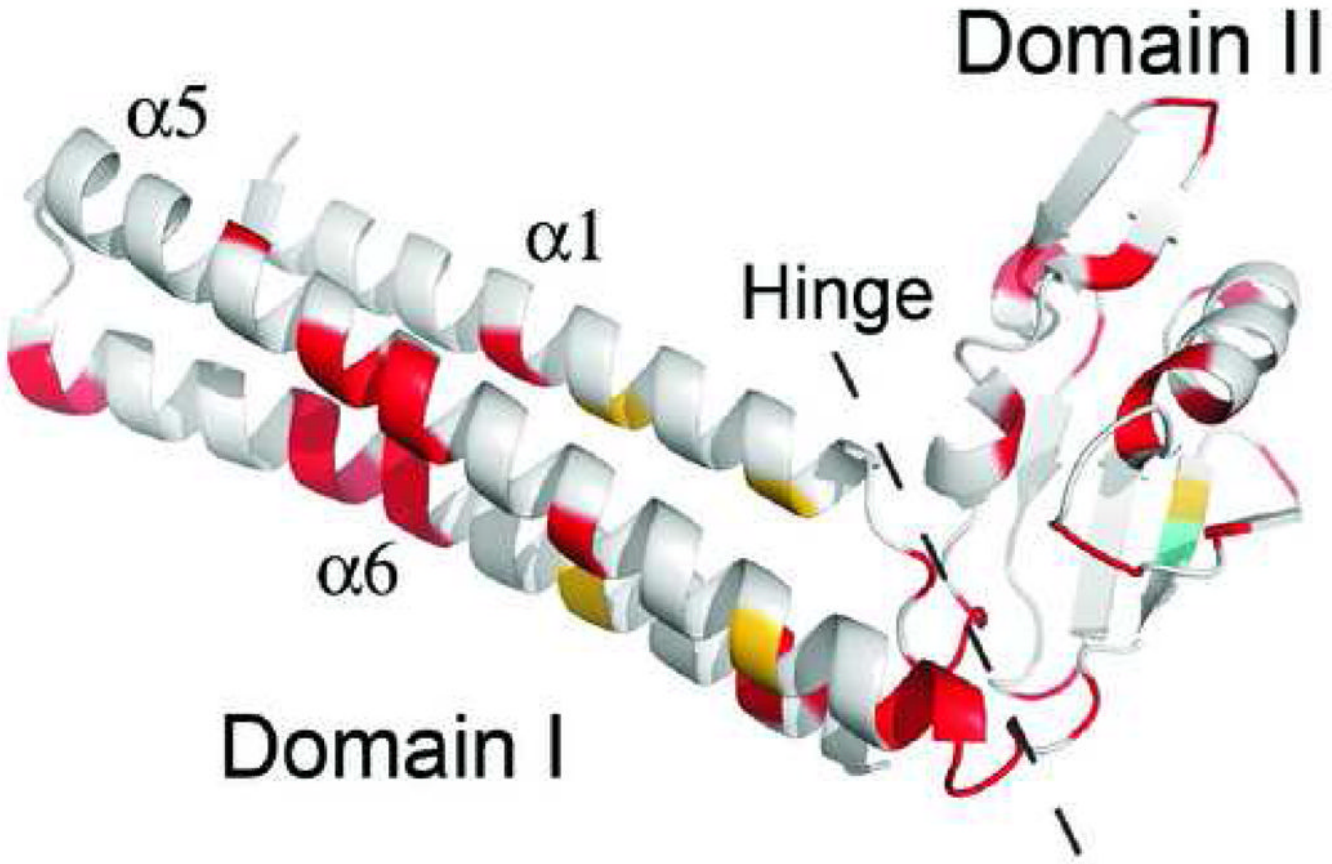

Figure 2. Structure of RRF

Crystal structure of *T. thermophilus* RRF (PDB ID: 1EH1)[19]. RRF Domain I consists of a 3-helix bundle (the five helices present in *T. thermophilus* RRF are designated as: α1, α5, and α6 according to the nomenclature derived from Selmer *et al.*[17]. Domain II consists of a β/α/β–sheet motif. The approximate location of the flexible hinge between RRF Domains I and II is indicated by the dotted line. For conserved amino acids in RRF across all species (Methods), those that are identical in both *E. coli* and *T. thermophilus* RRF are colored red, those that are similar in two species are colored gold, and those that are dissimilar in the two species are colored cyan. Amino acids in grey are not conserved in RRF.

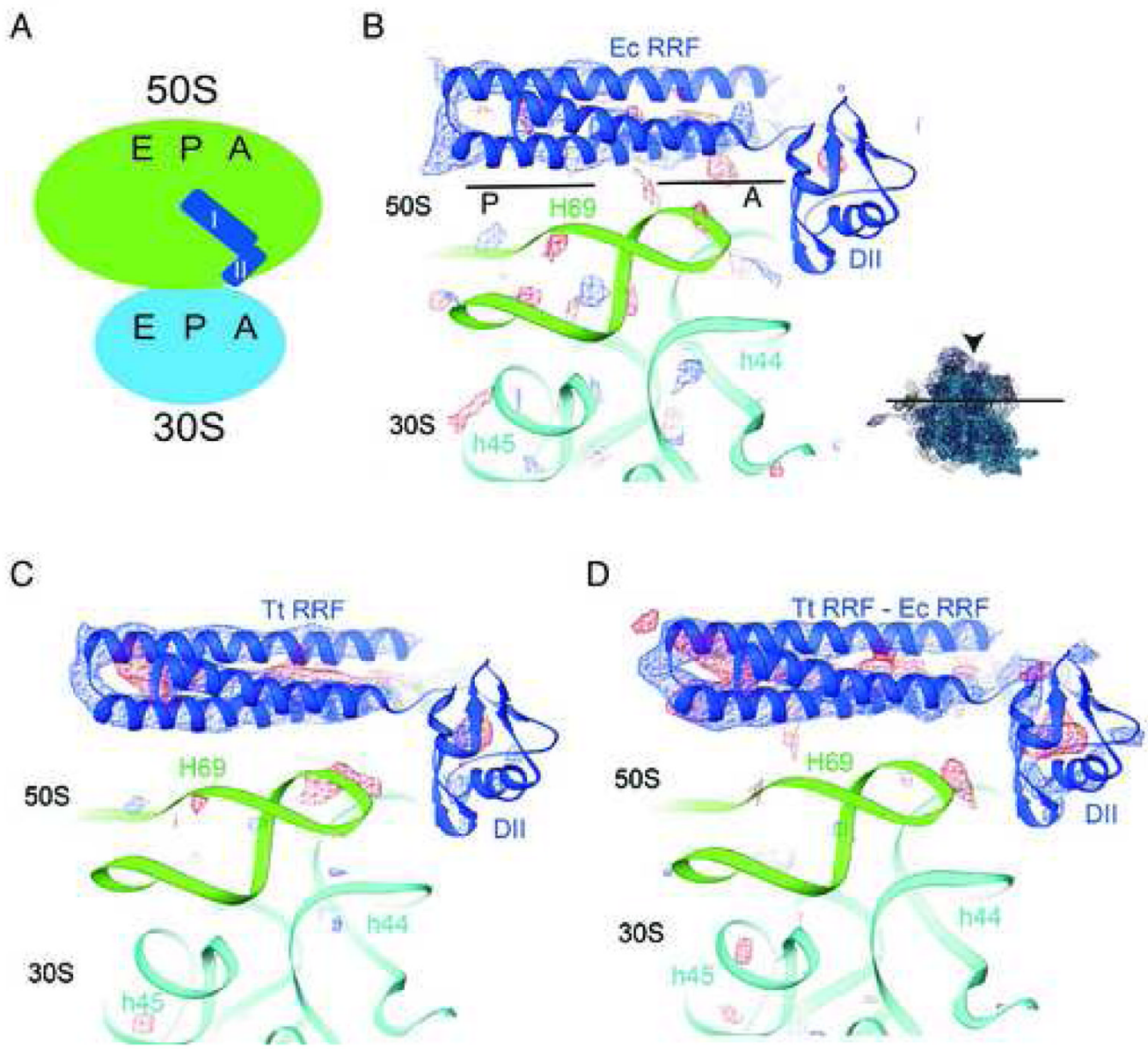

Figure 3. Comparison of *E. coli* RRF and *T. thermophilus* RRF binding to *E. coli* 70S ribosome II in pre-grown ribosome crystals

(A) Schematic representation of the 70S ribosome/RRF complex in the classical conformation, i.e. unratcheted state. All crystallographic analyses in this paper were performed on this complex. (B) F_{obs} - F_{obs} difference electron density map comparing the 70S ribosome/*E. coli* RRF complex to the apo-70S ribosome (Methods) is shown at 6 Å resolution. In this figure, *T. thermophilus* RRF (pdb ID: 1EH1)[19] is used as a homology model for *E. coli* RRF and is docked into the positive difference density. The approximate locations of the P site and A site are indicated by lines near H69 in the figure. (C) F_{obs} - F_{obs} difference electron density map comparing the 70S ribosome/*T. thermophilus* RRF complex to the apo-70S ribosome (Methods) is shown at 6 Å resolution. (D) F_{obs} - F_{obs} difference electron density map comparing the 70S ribosome/*T. thermophilus* RRF complex to the 70S ribosome/*E. coli* RRF complex at 6 Å resolution.

In panel (B), positive density (blue) and negative density (red) are at +/−2.5 standard deviations from the mean. In panels (C) and (D), positive density (blue) and negative density (red) are contoured at +/− 3 standard deviations from the mean, respectively. RRF is shown (blue), as are 16S rRNA (cyan) and 23S rRNA (green). The approximate location of RRF Domain II (DII) is shown. The direction of view is shown by the icon to the right in panel (B).

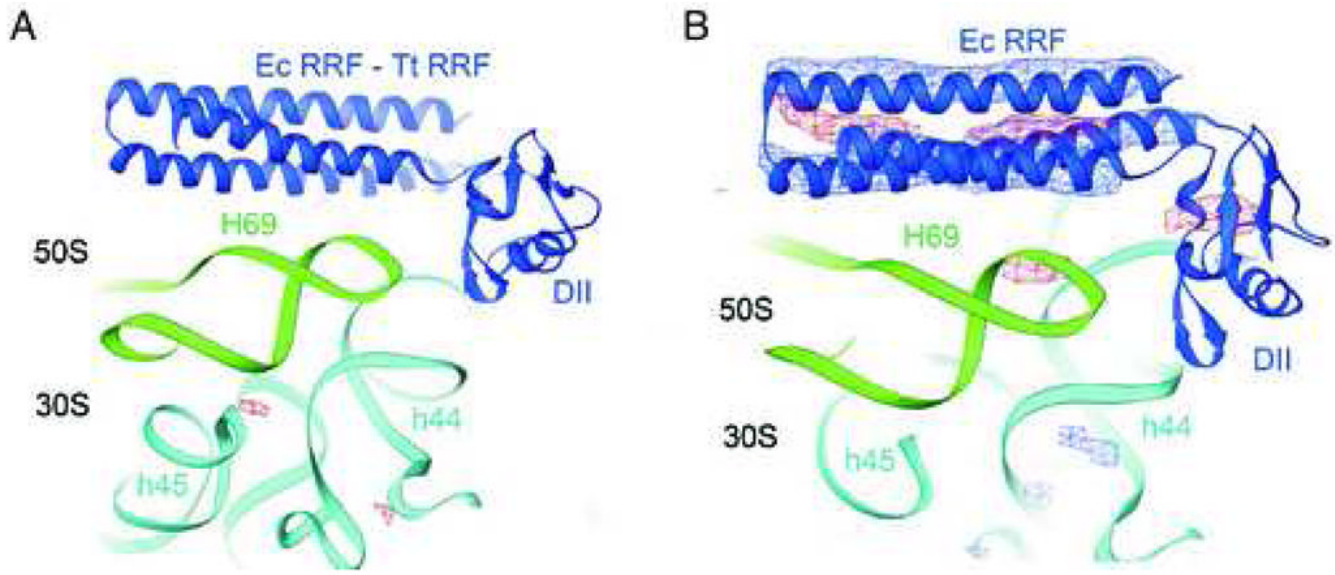

Figure 4. E. coli RRF in complex with ribosome II in crystals grown from pre-formed RRF ribosome complexes

(A) F_{obs} - F_{obs} difference electron density map comparing 70S ribosomes co-crystallized with *E. coli* RRF to 70S ribosomes in pre-grown crystals subsequently soaked with *T. thermophilus* RRF, at 8 Å resolution. Since no significant difference density is evident, the co-crystallized *E. coli* RRF 70S ribosome complex is nearly identical to the complex formed by soaking the RRF into the pre-formed crystals. (B) F_{obs} - F_{obs} difference electron density map comparing 70S ribosomes co-crystallized with *E. coli* RRF to the apo-70S ribosome, at 8 Å resolution. Positive density (blue) and negative density (red) are at +/− 3 standard deviations from the mean, respectively. Elements in the ribosome and RRF are colored as in Figure 3. The approximate location of RRF Domain II (DII) is shown. The direction of view is shown by the icon in Figure 3B.

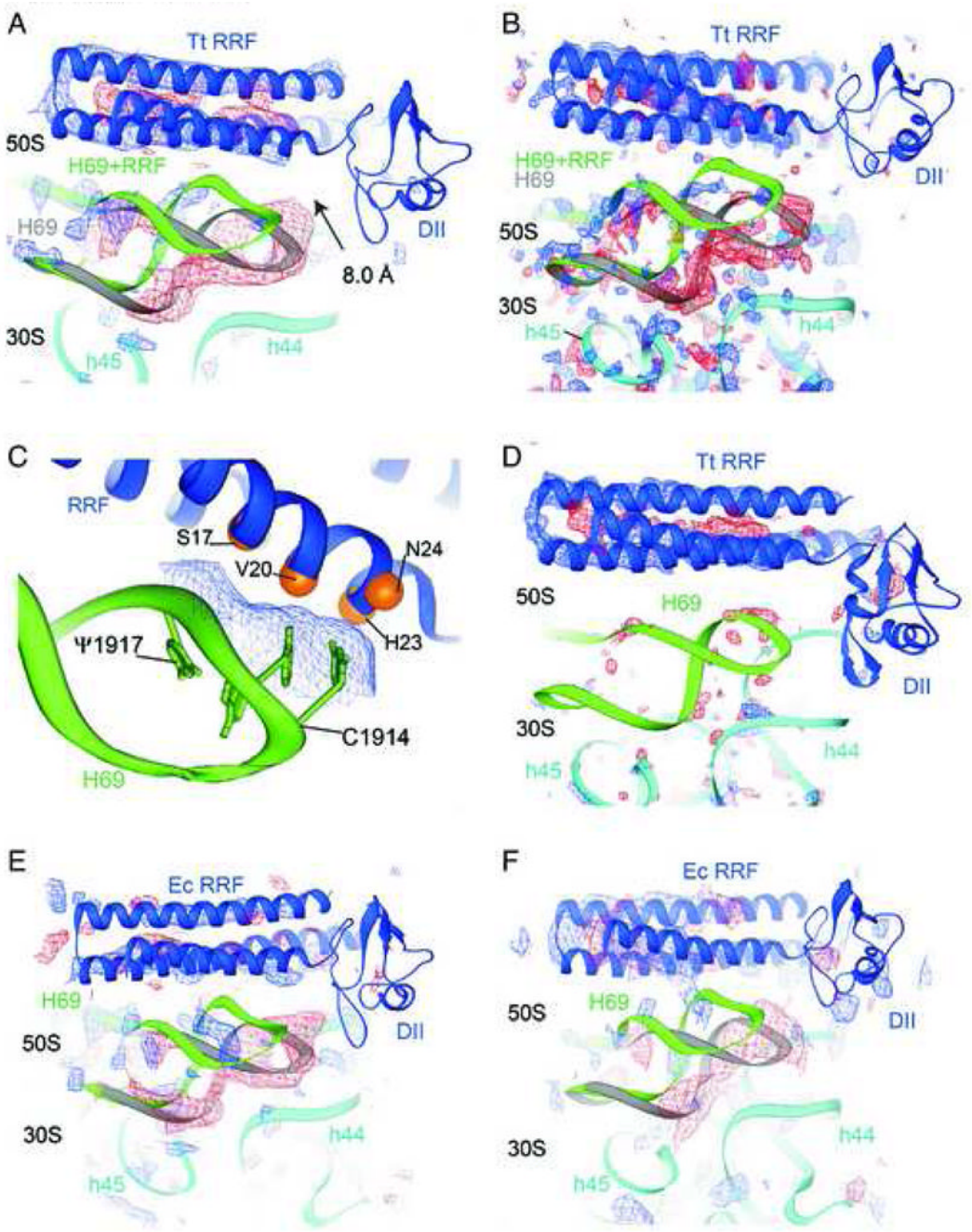

Figure 5. The movement of helix H69 upon RRF binding

(A) F_{obs} - F_{obs} difference electron density map comparing the 70S ribosome/*T. thermophilus* RRF complex to the apo-70S ribosome (ribosome I), at 6 Å resolution. (B) F_{obs} - F_{obs} difference electron density map comparing the 70S ribosome/*T. thermophilus* RRF complex to the apo-70S ribosome (ribosome I), at 3.5 Å resolution. (C) Close-up of interactions between H69-I and *T. thermophilus* RRF Domain I in ribosome I. The molecular surface of H69 at the interface with RRF is shown. The gold spheres are the Cα positions of the residues in RRF that likely contact H69. (D) F_{obs} - F_{obs} difference electron density map comparing the 70S ribosome/*T. thermophilus* RRF complex to the apo-70S ribosome (ribosome II) is shown, at 3.5 Å resolution. (E) F_{obs} - F_{obs} difference electron density map comparing the soaked 70S

ribosome/*E. coli* RRF complex to the apo-70S ribosome (ribosome I) is shown, at 6 Å resolution. (F) F_{obs} - F_{obs} difference electron density map comparing the co-crystallized 70S ribosome/*E. coli* RRF complex to the apo-70S ribosome (ribosome I) is shown, at 8 Å resolution.

In panels (A) and (B), positive density (blue) and negative density (red) are at +/−2.5 standard deviations from the mean, respectively. In panel (D), positive density (blue) and negative density (red) is contoured at +/− 3 standard deviations from the mean, respectively. In panels (E) and (F), positive density (blue) and negative density (red) are at +/− 2.2 standard deviations from the mean, respectively. Elements in the ribosome and RRF are colored as in Figure 3. The approximate location of RRF Domain II (DII) is shown. The direction of view is shown by the icon in Figure 3B.

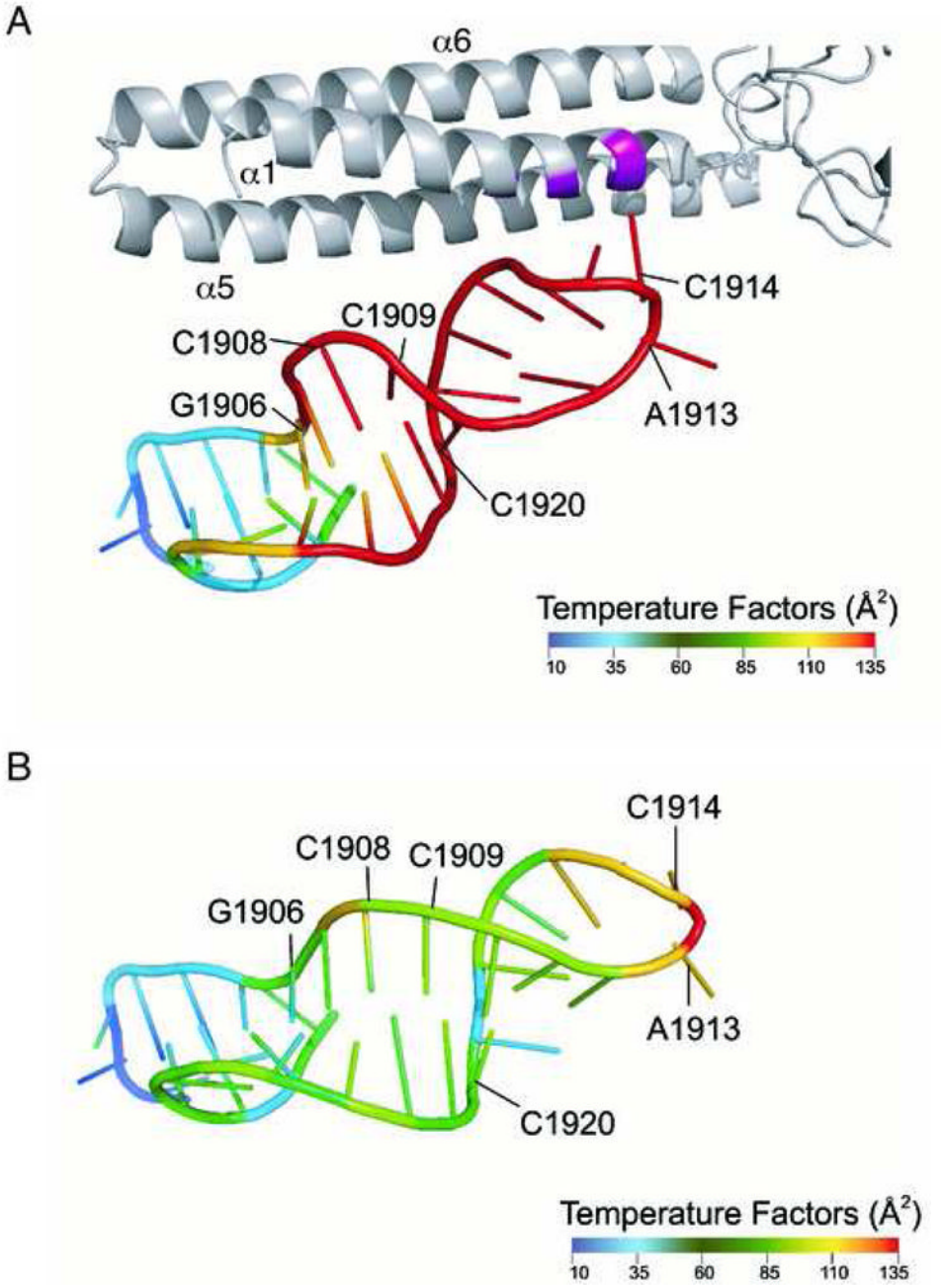

Figure 6. Temperature factors of helix H69-I in the 70S ribosome structures

(A) Temperature factors in H69-I in the 70S ribosome/*T. thermophilus* RRF complex. RRF is in grey with amino acids in close proximity to H69 highlighted in magenta. (B) Temperature factors in H69-I in the apo-70S ribosome[32].

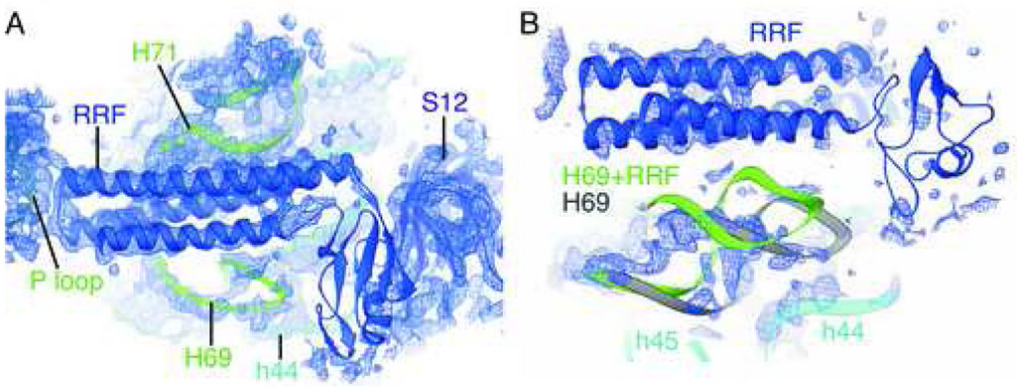

Figure 7. $3F_{obs}$ - $2F_{calc}$ electron density maps at 3.3 Å resolution detailing the interaction of *T. thermophilus* RRF Domain I with the ribosome

(A) *T. thermophilus* RRF Domain I docked into $3F_{obs}$ - $2F_{calc}$ difference electron density (blue), in ribosome II. (B) *T. thermophilus* RRF Domain I docked into $3F_{obs}$ - $2F_{calc}$ difference electron density (blue), in ribosome I. The position of Domain II is based on rigid-body refinement of the domain against the crystallographic data (see Methods). In panels (A) and (B), the electron density is contoured at +/− 1.2 standard deviations from the mean, respectively.

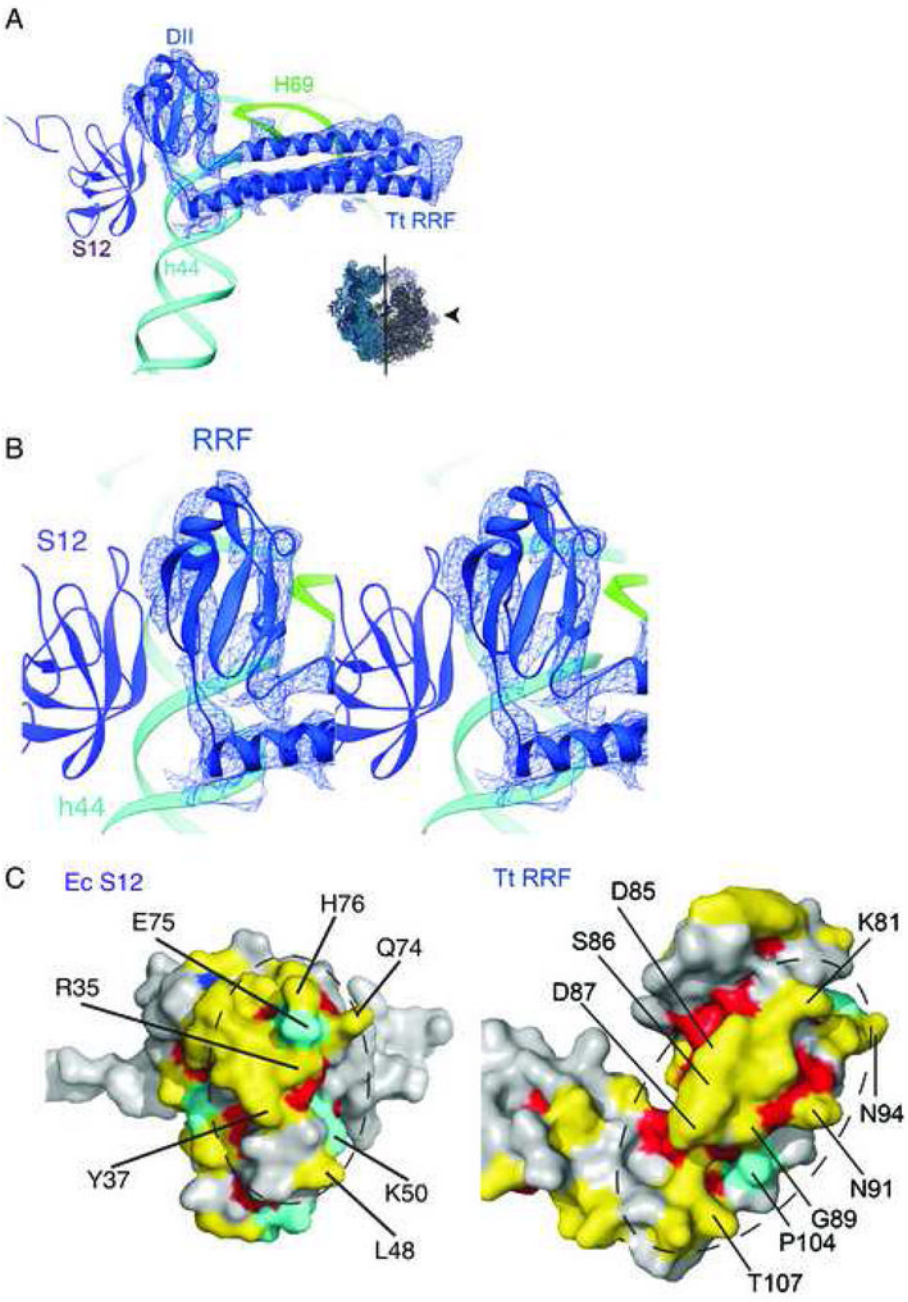

Figure 8. Interaction of RRF Domain II with protein S12

(A) F_{obs} -F_{obs} difference electron density map comparing the 70S ribosome/*T. thermophilus* RRF complex to the 70S ribosome/*E. coli* RRF complex (ribosome II), at 6 Å resolution. *T. thermophilus* RRF Domain II refined as a rigid body (Methods) is shown docked into the difference density. Ribosomal protein S12 (dark purple) and h44 in 16S rRNA (cyan) are also shown. Positive density (blue) near RRF is shown, at +2 standard deviations from the mean. The direction of view is shown by the icon to the right. (B) Stereo view of the interaction between *T. thermophilus* RRF Domain II and protein S12. (C) Evolutionary trace analysis of RRF and protein S12. The interaction in (A) has been "opened" to yield the surface interaface of S12 (left, same orientation as in panel A) and RRF (right, rotated 180° around the vertical

axis relative to panel A). Residues that are conserved and buried are colored dark blue on the molecular surface representations. Residues that are conserved and exposed are colored light blue. Residues that are class-specific and buried are colored red. Residues that are class-specific and exposed are colored gold. The approximate interface between *T. thermophilus* RRF Domain II and *E. coli* protein S12 is indicated by the dotted ellipses.

Table 1

Crystallographic statistics of diffraction data.

	T. thermophilus RRF	T. thermophilus RRF	E. coli RRF	E. coli RRF Co-crystal
Crystal growth conditions [Mg^{2+}]	33 mM	24 mM	24 mM	33 mM
RRF soaking time	3–4 d	12 h	12 h	N/A
Space group	$P2_12_12_1$	$P2_12_12_1$	$P2_12_12_1$	$P2_12_12_1$
Cell dimensions				
a	207.9	210.1	210.1	210.1
b	378.2	378.7	378.4	380.4
c	736.3	737.8	739.7	739.7
Resolution (Å) [high-resolution bin]	123-3.3 [3.55-3.3]	75.4-4.15 [4.22-4.15]	138-4.3 [4.37-4.3]	138-7.0 [7.12-7.0]
I/σI	12.5 [2.4]	7.0 [2.0]	6.48 [2.3]	8.0 [2.2]
Completeness %	96.8 [52.6]	79 [60]	94 [78.1]	71.4 [73]
Measurement Redundancy	4.6 [1.6]	2.4 [1.6]	3.3 [1.9]	4.1 [4.1]
R_{sym} or R_{merge}	10.4 [35.3]	8.4 [5.2]	15.2 [31.4]	19.2 [79.2]
Refinement Resolution (Å)	40-3.3			
No. of reflections	Total: 738,488	R-free: 35,383		
R_{work}/R_{free} (%)	27.5/30.4			
No. atoms	284,210			
Mean B-factor ($Å^2$)	69.7			
R.m.s deviations				
-Bond length (Å)	.003			
-Bond Angle (°)	.929			

Table 2

Table of Interactions of RRF Domain I with 23S rRNA

23S rRNA helix	23S rRNA nucleotide	RRF amino acid	Secondary structural Element in RRF
H69	Ψ1917	S17	α1
H69	A1916	V20	α1
H69	m^3Ψ1915	V20	α1
H69	C1914	H23	α1
H69	C1914	N24	α1
H71	C1947	R119	α5
H71	G1945	E123	α5
H71	U1946	E123	α5
H71	U1963	E123	α5
H71	U1946	R126	α5
H71	U1963	V127	α5
H71	C1942	R130 (R129)	α5
H71	U1943	R130 (R129)	α5
H71	G1945	R130 (R129)	α5
H71	C1941	R133 (R132)	α5
H71	C1942	R133 (R132)	α5
H71	C1965	R134 (R133)	α5
H71	C1942	Q162	α6
H71	U1943	D166	α6
P-loop	G2255	H148	α5- α6 loop
P-loop	G2255	L149	α5- α6 loop
P-loop	C2254	S150	α5- α6 loop
P-loop	G2253	E151	α5- α6 loop
P-loop	G2253	D152	α5- α6 loop

*(Amino Acids in parenthesis represent positions in *E. coli* RRF)

**Designation of the five αhelices in *T. thermophilus* RRF are based on nomenclature established by Selmer *et al.*[17]. See Figure 2 for positions of the corresponding α helices.